International Journal of Automotive Engineering, Vol. 8, No. 2, (2018), 2709-2729

Iran University of Science and Technology

International Journal of Automotive Engineering

Journal Homepage: ijae.iust.ac.ir

ISSN: 2008-9899

# Vertical Dynamics Modeling and Simulation of a Six-Wheel Unmanned Ground Vehicle

**Vahid Tavoosi [1*], Javad Marzbanrad [2], Ramadan Mirzaei [3]**

[1] Ph.D. Student, School of Automotive Engineering, Iran University of Science and Technology, Tehran, Iran

[2] Associate Professor, Vehicle Dynamical Systems Research Laboratory, School of Automotive Engineering, Iran University of Science and Technology, Tehran, Iran

[3] Assistant Professor, Department of Vehicle Science and Technology, Tehran, Iran

**ARTICLE INFO**

**Article history**:
Received : 11 Feb 2018
Accepted: 15 May 2018
Published:

**Keywords**:
Articulated suspension MULE;
Six-wheel vehicle Modeling;
Vertical dynamics Vibration;
Simulation Sensitivity analysis;

**A B S T R A C T**

Vertical dynamics modeling and simulation of a six-wheel unmanned military vehicle (MULE) studied in this paper. The Common Mobility Platform (CMP) chassis provided mobility, built around an advanced propulsion and articulated suspension system gave the vehicle ability to negotiate complex terrain, obstacles, and gaps that a dismounted squad would encounter. Aiming at modeling of vehicle vertical dynamics, basic and geometrical parameters defined and degrees-of-freedom specified on a compromise between accuracy and complexity of two models. Equations of motion provided on two linear and nonlinear 5-degree-of-freedom models using two different modeling methods. There is good agreement between time responses of two presented models. The main differences of two models observed in articulated suspension degrees-of-freedom while the vehicle subjected to high frequency maneuvers that cause severe oscillations on wheels and arms in comparison to vehicle body due to lower mass and inertia properties. The linear model can be used to design a controller and the nonlinear to predict vehicle motion more accurately. Sensitivity analysis of the influential parameters is also presented to specify effects of different parameters. Results of this study may be used to design articulated suspension and making next frequency analyses.

*Corresponding Author
Email Address:
v_tavoosi@auto.iust.ac.ir



[ DOI: 10.22068/ijae.8.2.2709 ]

## 1. Introduction

A series of military vehicles called "unmanned vehicles" are used to increase the safety of soldiers, the speed of the transfer and relocation of logistics, the speed of clearing contaminated areas, the speed of various operations, the amount of equipment, and, ultimately, the support of operational areas. By employing these unmanned military vehicles, it will be possible to detect, convey, attack and decisively finish pre-enemy operations [1]. These vehicles can be sheltered in safe areas by providing remote control and can be called up quickly if needed [2]. Unmanned military vehicles require different technologies in areas such as communication, mobility, power transmission, preservation, and the interaction between robots and humans.

One of the most famous cars of this family is known as MULE. The three main types of this vehicle are: transport vehicles, antique cars and armed robotic vehicles [3]. The MULE comes with a simple chassis for loading, an articulated suspension system and an advanced propulsion engine that allows you to navigate at very uneven surfaces, barriers and holes in the pedestrians facing operational areas. The unique and advanced suspension system of the vehicle, coupled with in-hub motors powering each wheel, has many advantages over conventional suspension systems and allows it to maneuver over a wide range of conditions and obstacles ahead of the vehicle. For example, it can cross steps up to 1 meter, a transverse gradient of 40%, water-filled passages to a depth of 0.5 m, and passing through obstacles up to 0.5 m without colliding to it. The car can correct the suspension state by loading and location of the center of mass to achieve optimal performance and carry up to 1,100kg of load [4]. The maximum speed is also 70 km / h in rugged areas [2]. MULE can also be used as a power source for battery charging and power generation [5]. The car also features multiple sensors with night and day functionality, infrared equipment, barrier detection, and the identification of chemical and biological compounds in operational areas [6].

In a categorization, suspension systems fit into one of the groups; rigid, independent, articulated, rocker-buggy, segmented-body rovers, and active suspension, an articulated type is the subject if of this study. So far, several robots and rovers have been introduced using articulated suspension systems. But they generally have special applications and are not designed for difficult situations and movements in impassable areas.

Independent articulated mechanisms for use in the suspension system can have different degrees of freedom. In Figure 2, four examples of these mechanisms are displayed. The articulated mechanism (a) has three degrees of freedom, and due to its slippage, its components are required to enhance the rigidity of the assembly. The articulated mechanism (b) has the ability to change the length of the main suspension arm. The articulated mechanism (c) is another type of mechanism (b) having a deviation angle $\alpha$ relative to the main axis of suspension. The other type of hinge mechanism will be in the form (d), which will allow the suspension arm to be circular along the way, and will make it easier and more robust and more resistant to previous mechanisms and is more suitable for high-speed applications such as vehicles.

Seidla [9] examines a four-wheeled car with an articulated suspension mechanism and points out that without an articulated suspension system there will be no possibility of passing through high-altitude obstacles, because after passing the front wheels on the obstacle, the load will be transferred to rear wheels, and front wheels do not have enough traction to raise the rear wheels. It should be noted that the rear tires are able to provide thrust to the separation point, and then the front tires must provide the thrust necessary to raise the vehicle.



[ DOI: 10.22068/ijae.8.2.2709 ]

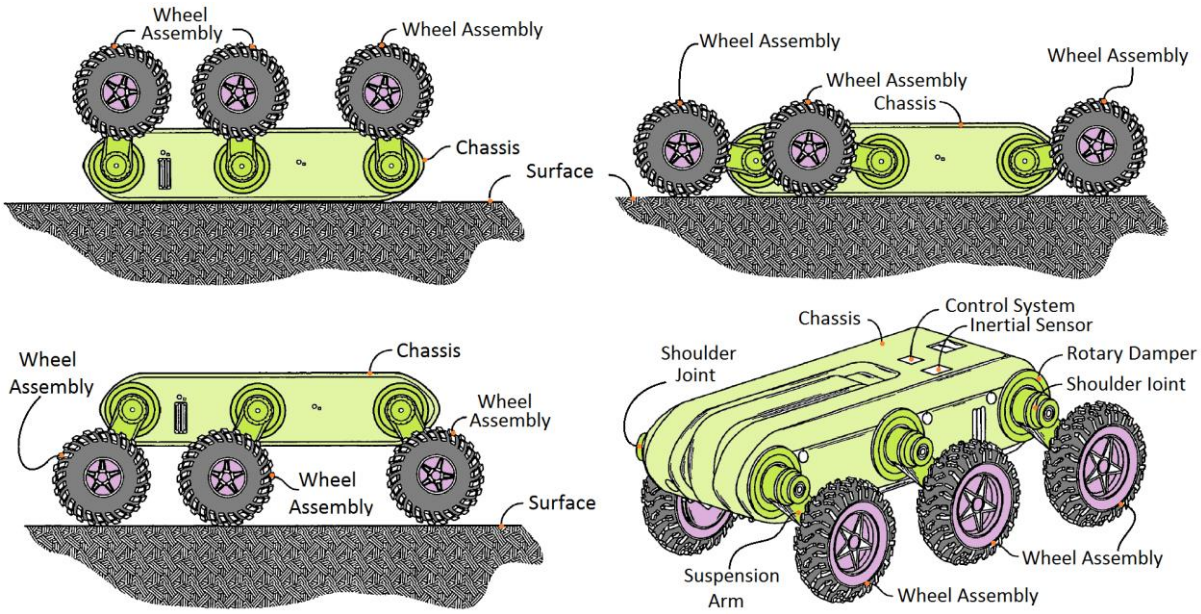


Figure 1 - Main components of the MULE vehicle and different modes of changing the angle of the suspension system [7]

If the center of mass moves to the front, the vehicle can cross the barrier. This requires the use of a mechanism to change the location of the center of mass. If the articulated suspension mechanism is used, the center of the mass will be tilted backward when the front wheels reach the obstacle, thereby this increases the traction of the rear wheels and subsequently the driving force of the front wheel and allows the rover to pass the obstacle. The height of the passable obstacle is depended on the length of the arms and the minimum ground clearance. Whenever there are four wheels for the rover, passing an obstacle may cause rollover, and with the help of six wheels, it can pass the obstacles more steadily and successfully.

There are also several types of Rocker Boogie system designed to overcome obstacles at low speeds, with the mechanism of rotation and wheel movement, similar to those equipped with an articulated suspension system that was discussed earlier.

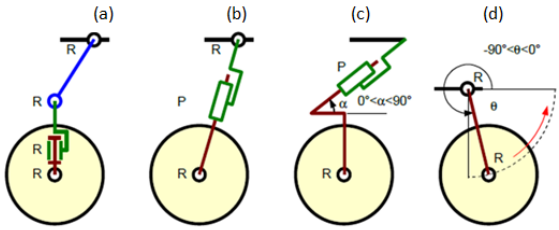


**Figure 2**. Various types of arms for using in independent hinged suspension [8]

But there are differences in terms of mechanism, control and movement. This system can provide the possibility of crossing obstacles to an approximate height of the wheel radius. To overcome obstacles, the rover shall stop completely and the obstacle passes slowly, to minimize the dynamic impact on the suspension system. This system is used in sample of mars rover. The main disadvantage is the low speed of vehicles that use such a system. In this design, the suspension system will go through two stages and will gradually cross the obstacles. To cross the obstacle, the front wheels are pushed by the rear and center wheels force, and the wheel passes through the obstacle as a result of a slow turning of the front wheel. Then the



[ DOI: 10.22068/ijae.8.2.2709 ]

middle wheels are pressed against the obstacle by the rear wheels and pass through it. In the further, the rear wheels with a thrust on the front and center wheels climb the obstacle and the vehicle completely passes. When the front wheel is obstructed, the speed of the rover wheels are the same, but suddenly the center wheels speed increase and the rear wheels speed drop. When the front wheel has reached the top of the barrier, the speed of the all wheels will be the same again. The same strategy will be used for the middle wheel [11]. NASA has also developed other variants [12, 13], in which two wheels are mounted on a Rocker and a wheel is attached to a boom, and one side bogie is connected to the other side bogie with a hinged link.

In 2013, Avinash et al. [14] designed a semi-active small robot to cross the barrier with a type of articulated suspension system. The main feature of this sample is that it acts inactive when passing through low-altitude obstacles and only uses its motors to cross high-rise obstacles. Another advantage is that it doesn't need information about the obstacle and automatically detects function (active or inactive) of passing the obstacle. The suspension of the robot is rigid for each axle and the axles are connected to each other using hinged joints. Another example of the articulated suspension system is introduced to use on rugged surfaces for military vehicles and rovers [15]. In this suspension system, vehicle control is performed using the tire and surface contact angle. Among other robots made with other types of hinged technology, Octopus [16], Sojourer [17], Hybtor [18], Nomad [19] and Marsokhod [20] are mentioned.

In the study of the dynamics of articulated suspension vehicles, Lim et al. [21], in the field of steering wheel control, have provided a method for controlling the MULE suspension system, which does not require the availability of details of surface geometry and ground effects. Surface roughnesses are estimated by tracking the movement of each wheel, and a predetermined plan for the suspension system behavior when crossing the roughnesses. Kang et al.[22-24] also examined the longitudinal and transverse dynamics of the vehicle to control the steering system. The model provided for the vehicle consists of three separate sections. The model of the actuator system (including wheels and propulsion), the model of the suspension arm assembly, which will be simultaneously solved for each arm, and ultimately the body model of the car, each one in a relationship with each other. This model incorporates the longitudinal and lateral body dynamics simultaneously and the dynamics of the arms is also studied in longitudinal, transverse, and vertical directions.

In 2002, Bares et al. [25] developed an articulated suspension system for the Spinner vehicle that uses the hydropneumatic return mechanism. In this mechanism, the oil moves from the inside of the damper and pushes it to the separator, which plays the role of the spring mechanism. This mode of operation creates a spring with variable rigidity, which is very suitable for moving in rugged roads. The height of the suspension arm is adjustable by transferring oil from one cylinder to the other cylinder.

Due to the high power loss in skid steering systems, Fauroux et al. [26] conducted a study to improve the skid steering system of a six-wheeler, with an independent articulated suspension system. The control of the vertical load of tires in their study has been considered, and by adjusting the angle of the suspension arms, improvements in power consumption have been given. Ultimately, the power consumption has dropped by about 20-30%. Its suspension angles are limited and have a special motion mechanism that is different from military vehicles. The vehicle propulsion is of the belt driven type and the power of each wheel is provided by an independent belt system. On the other hand, the height



[ DOI: 10.22068/ijae.8.2.2709 ]

adjustment of the suspension system is also possible with hydropneumatic springs. In another study, Mohammad Javad [27] studied the transverse dynamics of a six-wheeled ATV class vehicle to control the skid steering system. The simultaneous use of sensors mounted on the vehicle and methods for estimating the status variables are used in his study.

So far, studies of the vibrational motion of hinged suspension vehicles have been done by some researchers. The use of an articulated suspension system for vehicles and rover with the ability to navigate in rugged roads will be inevitable. Consequently, Sanan et al. [28] examined the motion of a vehicle with an articulated suspension system on rugged roads. Creating and controlling the appropriate contact force for moving vehicles at these levels is one of the most basic issues. For this purpose, the focus is on wheel dynamics and the suspension arm of an articulated active suspension system that has been modeled as a linear spring-damper assembly and the body dynamics has been neglected. In a more detailed study, Eathakota et al. [29] have investigated a linear articulated suspension system and presented strategies for controlling tire contact force on the road surface. The model presented in their study was semi-static. A model for calculating thrust forces for each wheel has also been presented in their study.

The proposed vehicle has unique features that give it a vast operational capability. The main and most important part of the vehicle is the suspension system. The suspension system varies with conventional models and has many complexities. The articulated suspension system used in addition to mechanical mechanisms are accompanied by advanced electric motors that are used to steer, drive, brake, control vibrations and adjust the height. Providing a model of the vehicle suspension to simulate its movement in maneuvers and finally producing it is very important. Therefore, the dynamics of the suspension system will be discussed in this paper, in order to carry out the expected requirements of the vehicle when passing through rugged roads. Accordingly, dynamics modeling and simulation of the vehicle will focus on the suspension system.

## 2. Modeling

Modeling of vibrational motion of studied vehicle will be done in two linear and nonlinear modes in two different ways. Both models have 5 degrees of freedom, including 3 degrees of freedom related to the angular motion of the suspension arms, a degree of freedom for pitch angle of the body, and a degree of freedom related to the vertical displacement of the body. According to this description, it is assumed that the road input is equal in both right and left sides of the vehicle. Also, the effect of weight forces is not included in the model directly. Because it is assumed that the forces of weight and elasticity of the system neutralize each other and make the initial conditions of the vehicle suspension. It should be noted that the effect of weight forces will be important when calculating the static load of each wheel of a vehicle and will be addressed in a separate section.

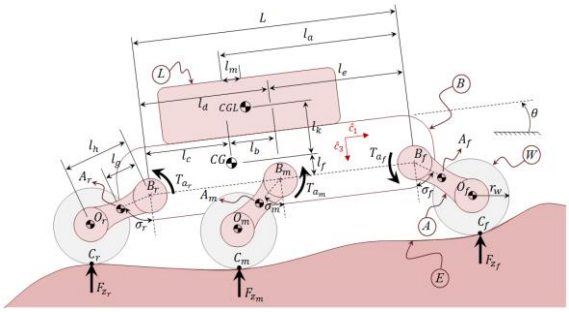

**Figure.3** Vehicle free body diagram and its geometric parameters

The free body diagram of the vehicle and its geometric parameters are shown in Figure. 3. The torque exerted on the suspension arms and





[ DOI: 10.22068/ijae.8.2.2709 ]

the vertical forces of the road, which are marked with respectively $T_a$ and $F_z$, change the dynamics of the vehicle. The value of these two quantities can be calculated using the linear and rotational displacements of the system and the use of defined elasticity. For all of kinematic and kinetic parameters, the index *f*, *m*, and *r* represent, respectively, the front, center and rear wheels. Reference frameworks E, A, W, B and L are fixed on the ground, suspension arm, wheel, body, and load, respectively.

Body center of mass, loads, suspension arms, and wheels are displayed respectively with *CG*, *CGL*, *A* and *O*. The center of tire contact with the road and the center of the suspension arm are also marked with C and B, which also have indexes for each wheel. The initial deviation of each arm from the vertical axis of the body, is shown, with $\sigma$, that is chosen the same for all three suspensions at the start of the movement. The longitudinal distances $l_a$, $l_b$, $l_c$ ،$l_d$ and $l_e$ respectively indicate the longitudinal distance between the center of mass of the body to the center of the front arm, the longitudinal distance between the center of mass of the body to the center of rotation of the middle arm, the longitudinal distance between the center of mass of the body to the center of rotation of the rear arm, The longitudinal distance between the center of rotation of rear arm to the middle, and the longitudinal distance between the center of rotation of the middle arm to the front. Also, the vertical distance between the center of mass of the body and the axis passing through the centers of rotation of the arms, the distance between the center of mass of each arm to its center of rotation, the length of the suspension arm, the vertical distance between the center of mass of the body and the center of mass of load, respectively, with $l_f, l_g$، $l_h$ And $l_k$ are displayed. The longitudinal distance of the center of mass of the load to the center of mass of the body is shown by the parameter $l_m$. The total distance between the front and rear arms is obtained from the sum of the distances $l_e$ and $l_d$ and will be shown in relations with L. The effective wheel radius is also marked with $r_w$. Unit vectors attached to the center of mass of the body are also represented by $\hat{c}_1$, $\hat{c}_2$and $\hat{c}_3$, which are located in three directions, longitudinal, transverse, and vertical respectively. The system state variables are shown in Figure 4.

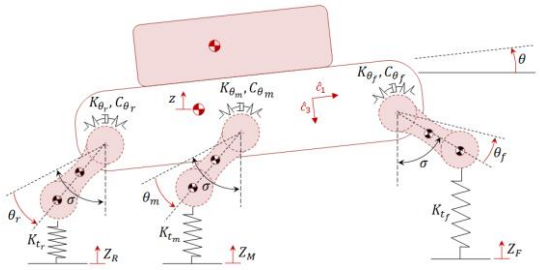


**Figure 4**. State parameters of vehicle vibration model

The road input to the front, middle and rear wheels is $Z_F$, $Z_M$ and $Z_R$ respectively, which can be calculated according to the speed of the vehicle for each wheel. The general relationship for the front wheel input is in equation (1).

$$Z_F = Z_0 \sin[\omega_0 t] \quad (1)$$

that by considering the geometric distance between each of the two tire contact centers and knowing the vehicle speed, it can be extended to the middle and rear wheels. In equation (1), $Z_0$ is the value of the road input amplitude and $\omega_0$ is the input frequency.

Each vehicle tire has a stiffness of $K_t$. The risen force between road and tires changes the angle of the front, middle and rear suspension arms with the angles $\theta_f$, $\theta_m$ and $\theta_r$. It should be noted that the instantaneous angle of each suspension arm is the sum of the angular variations and the initial value of $\sigma$. Each of the suspended arms has a torque at the point of hinge, due to the torsional stiffness and damping. The stiffness and damping of these connections are defined by $K_\theta$ and $C_\theta$. The





[ DOI: 10.22068/ijae.8.2.2709 ]

vertical displacement of the body will be shown by *z* parameter and the sliding angle is also shown with $\theta$. The symbols used in the two recent forms will be valid for both linear and nonlinear models.

### 2.1. Nonlinear model

For nonlinear model of vehicle vibrations, the Kane Dynamic method [30] is used, which is a suitable method for studying the dynamics of multi-body systems. In this method, it is necessary to determine the speed and acceleration of all the important points of the vehicle, including the mass centers, the contact patches, locations of forces and external torques. On the other hand, equations of motion will be obtained by specifying external forces and forces of moments and inertia. Inertial forces can be calculated using acceleration of different parts. The sum of two mentioned forces must be zero. All equations of motion will be derived from that equilibrium.

External forces applied by the road can be calculated according to the tire stiffness coefficient and displacement of wheel centers. If these forces are assumed to be in the vertical direction (ground coordinate system) of the vehicle, then these equation can be written:

$$\bar{F}_{Z_f} = -2K_{tf}\left(Z_F - Z_{O_f}\right)(\cos\theta\,\hat{c}_3 - \sin\theta\,\hat{c}_1) \quad (2)$$

$$\bar{F}_{Z_m} = -2K_{tm}(Z_M - Z_{O_m})(\cos\theta\,\hat{c}_3 - \sin\theta\,\hat{c}_1) \quad (3)$$

$$\bar{F}_{Z_r} = -2K_{tr}(Z_R - Z_{O_r})(\cos\theta\,\hat{c}_3 - \sin\theta\,\hat{c}_1) \quad (4)$$

Where $Z_O$ represents the vertical displacement of the center of each wheel. For each front, center, and rear wheel center, there will be:

$$Z_{O_f} = \{z + l_a \sin\theta + l_f(1-\cos\theta) - l_h[\cos(\sigma+\theta+\theta_f) - \cos\sigma]\} \quad (5)$$

$$Z_{O_m} = \{z + l_b \sin\theta + l_f(1-\cos\theta) - l_h[\cos(\sigma-\theta-\theta_m) - \cos\sigma]\} \quad (6)$$

$$Z_{O_r} = \{z - l_c \sin\theta + l_f(1-\cos\theta) - l_h[\cos(\sigma-\theta-\theta_r) - \cos\sigma]\} \quad (7)$$

The amount of external torque at the point where the suspension arms are attached to the body will also be determined using the following equation. Given the fact that the vehicle is symmetrical, external torques and forces are doubled and may be as:

$$\bar{T}_{a_i} = 2(K_{\theta i}\theta_i + C_{\theta i}\dot{\theta}_i)\hat{c}_2 \quad ; \quad i = f, m, r \quad (8)$$

Accordingly, the first equation concerning the degree of freedom of vertical body movement is:

$$\begin{aligned}\ddot{z}\{m_b + m_L + 6m_a + 6m_w\} &+ \ddot{\theta}\{l_m m_L + 2(l_a + l_b - l_c)(m_a + m_w) + 2(m_a l_g + m_w l_h)[\sin(\sigma+\theta_f) - \sin(\sigma-\theta_m) - \sin(\sigma-\theta_r)]\} \\ &+ 2\ddot{\theta}_f\{(m_a l_g + m_w l_h)\sin(\sigma+\theta_f)\} \\ -2\ddot{\theta}_m\{(m_a l_g + m_w l_h)\sin(\sigma-\theta_m)\} \\ -2\ddot{\theta}_r\{(m_a l_g + m_w l_h)\sin(\sigma-\theta_r)\}\end{aligned} \quad (9)$$





[ DOI: 10.22068/ijae.8.2.2709 ]

$$
\begin{aligned}
&= 2\cos\theta\left\{K_{tf}\left(Z_F - Z_{O_f}\right)\right. \\
&\qquad + K_{tm}\left(Z_M - Z_{O_m}\right) \\
&\qquad \left. + K_{tr}\left(Z_R - Z_{O_r}\right)\right\} \\
&-2\left(\dot{\theta} + \dot{\theta}_f\right)^2\left(m_a l_g\right. \\
&\qquad \left. + m_w l_h\right)\cos\left(\sigma\right. \\
&\qquad \left. + \theta_f\right) \\
&-2\left(\dot{\theta} + \dot{\theta}_m\right)^2\left(m_a l_g\right. \\
&\qquad \left. + m_w l_h\right)\cos(\sigma \\
&\qquad - \theta_m) \\
&-2\left(\dot{\theta} + \dot{\theta}_r\right)^2\left(m_a l_g\right. \\
&\qquad \left. + m_w l_h\right)\cos(\sigma \\
&\qquad - \theta_r) \\
&-U\dot{\theta}\{m_b + m_L + 6m_a + 6m_w\} \\
&-\dot{\theta}^2\{-l_k m_L + 6l_f(m_a + m_w)\}
\end{aligned}
$$

Where $m_a$, $m_w$, $m_b$, $m_L$ determine the mass of each suspension arm, wheel, body and load of the vehicle, respectively. The vehicle longitudinal speed is also marked with *U*.

The next equation is related to pitch angel:

$$
\begin{aligned}
&\ddot{z}\{l_m m_L + 2(l_a + l_b - l_c)(m_a + m_w) \\
&\qquad + 2\left(m_a l_g\right. \\
&\qquad \left. + m_w l_h\right)\left[\sin\left(\sigma + \theta_f\right)\right. \\
&\qquad - \sin(\sigma - \theta_m) \\
&\qquad \left. - \sin(\sigma - \theta_r)\right]\} \\
&+\ddot{\theta}\{m_L(l_k^2 + l_m^2) + I_{yb} + I_{yL} + 6I_{ya} \\
&\qquad + 6I_{yw} \\
&\qquad + 2(m_a + m_w)\left(l_a^2\right. \\
&\qquad \left. + l_b^2 + l_c^2 + 3l_f^2\right) \\
&\qquad + 6\left(m_a l_g^2 + m_w l_h^2\right) \\
&\qquad + 4\left(m_a l_g\right. \\
&\qquad \left. + m_w l_h\right)\left[l_f\cos\left(\sigma\right.\right. \\
&\qquad \left. + \theta_f\right) \\
&\qquad + l_a\sin\left(\sigma + \theta_f\right) \\
&\qquad + l_f\cos(\sigma - \theta_m) \\
&\qquad - l_b\sin(\sigma - \theta_m) \\
&\qquad + l_f\cos(\sigma - \theta_r) \\
&\qquad \left. + l_c\sin(\sigma - \theta_r)\right]\}
\end{aligned}
\tag{10}
$$

$$
\begin{aligned}
&+2\ddot{\theta}_f\{I_{yw} + I_{ya} + \left(m_a l_g^2 + m_w l_h^2\right) \\
&\qquad + \left(m_a l_g\right. \\
&\qquad \left. + m_w l_h\right)\left[l_f\cos\left(\sigma\right.\right. \\
&\qquad \left. + \theta_f\right) \\
&\qquad \left. + l_a\sin\left(\sigma + \theta_f\right)\right]\} \\
&+2\ddot{\theta}_m\{I_{yw} + I_{ya} \\
&\qquad + \left(m_a l_g^2 + m_w l_h^2\right) \\
&\qquad + \left(m_a l_g\right. \\
&\qquad \left. + m_w l_h\right)\left[l_f\cos(\sigma\right. \\
&\qquad - \theta_m) \\
&\qquad \left. - l_b\sin(\sigma - \theta_m)\right]\} \\
&+2\ddot{\theta}_r\{I_{yw} + I_{ya} + \left(m_a l_g^2 + m_w l_h^2\right) \\
&\qquad + \left(m_a l_g\right. \\
&\qquad \left. + m_w l_h\right)\left[l_f\cos(\sigma\right. \\
&\qquad - \theta_r) \\
&\qquad \left. + l_c\sin(\sigma - \theta_r)\right]\} \\
&= 2K_{tf}\left(Z_F - Z_{O_f}\right)\{l_f\sin\theta + l_a\cos\theta \\
&\qquad + l_h\sin\left(\sigma + \theta + \theta_f\right)\} \\
&+2K_{tm}\left(Z_M - Z_{O_m}\right)\{l_f\sin\theta + l_b\cos\theta \\
&\qquad - l_h\sin(\sigma - \theta \\
&\qquad - \theta_m)\} \\
&\qquad + 2K_{tr}\left(Z_R\right. \\
&\qquad \left. - Z_{O_r}\right)\{l_f\sin\theta \\
&\qquad - l_c\cos\theta \\
&\qquad - l_h\sin(\sigma - \theta - \theta_r)\} \\
&-2\left(\dot{\theta} + \dot{\theta}_f\right)^2\left(m_a l_g\right. \\
&\qquad \left. + m_w l_h\right)\left[l_a\cos\left(\sigma\right.\right. \\
&\qquad \left. + \theta_f\right) \\
&\qquad \left. - l_f\sin\left(\sigma + \theta_f\right)\right] \\
&-2\left(\dot{\theta} + \dot{\theta}_m\right)^2\left(m_a l_g\right. \\
&\qquad \left. + m_w l_h\right)\left[l_b\cos(\sigma\right. \\
&\qquad - \theta_m) \\
&\qquad \left. + l_f\sin(\sigma - \theta_m)\right] \\
&+2\left(\dot{\theta} + \dot{\theta}_r\right)^2\left(m_a l_g\right. \\
&\qquad \left. + m_w l_h\right)\left[l_c\cos(\sigma\right. \\
&\qquad - \theta_r) \\
&\qquad \left. - l_f\sin(\sigma - \theta_r)\right]
\end{aligned}
$$



[ DOI: 10.22068/ijae.8.2.2709 ]

$$+\dot{z}\dot{\theta}\{-l_k m_L + 6l_f(m_a + m_w) + 2(m_a l_g + m_w l_h)[\cos(\sigma + \theta_f) + \cos(\sigma - \theta_m) + \cos(\sigma - \theta_r)]\}$$

$$-U\dot{\theta}\{l_m m_L + 2(m_a + m_w)(l_a + l_b - l_c) + 2(m_a l_g + m_w l_h)[\sin(\sigma + \theta_f) - \sin(\sigma - \theta_m) - \sin(\sigma - \theta_r)]\}$$

$$+2\dot{\theta}^2(m_a l_g + m_w l_h)\{l_a \cos(\sigma + \theta_f) + l_b \cos(\sigma - \theta_m) - l_c \cos(\sigma - \theta_r)\}$$

$$-2l_f\dot{\theta}^2(m_a l_g + m_w l_h)\{\sin(\sigma + \theta_f) - \sin(\sigma - \theta_m) - \sin(\sigma - \theta_r)\}$$

In the above equation $I_{ya}$, $I_{yw}$, $I_{yb}$, and $I_{yL}$, respectively, show the suspension arm, wheel, body, and load around the transverse axis, respectively. The third equation for the degree of freedom of the front suspension arms can be written as follows.

$$2\ddot{z}\{(m_a l_g + m_w l_h)\sin(\sigma + \theta_f)\} + 2\ddot{\theta}\{I_{yw} + I_{ya} + (m_a l_g^2 + m_w l_h^2) + (m_a l_g + m_w l_h)[l_f \cos(\sigma + \theta_f) + l_a \sin(\sigma + \theta_f)]\} + 2\ddot{\theta}_f\{I_{yw} + I_{ya} + (m_a l_g^2 + m_w l_h^2)\} = 2l_h K_{tf}\left(Z_F - Z_{O_f}\right)\sin(\sigma + \theta + \theta_f) - 2K_{\theta f}\theta_f - 2C_{\theta f}\dot{\theta}_f + 2\dot{z}\dot{\theta}\{(m_a l_g + m_w l_h)\cos(\sigma + \theta_f)\} - 2U\dot{\theta}\{(m_a l_g + m_w l_h)\sin(\sigma + \theta_f)\} + 2\dot{\theta}^2(m_a l_g + m_w l_h)\{l_a \cos(\sigma + \theta_f) - l_f \sin(\sigma + \theta_f)\} \quad (11)$$

The fourth equation regarding the degree of freedom of rotation of the middle suspension arms is:

$$2\ddot{z}\{(m_a l_g + m_w l_h)\sin(\sigma - \theta_m)\} + 2\ddot{\theta}\{I_{yw} + I_{ya} + (m_a l_g^2 + m_w l_h^2) + (m_a l_g + m_w l_h)[l_f \cos(\sigma - \theta_m) - l_b \sin(\sigma - \theta_m)]\} - 2\ddot{\theta}_m\{I_{yw} + I_{ya} + (m_a l_g^2 + m_w l_h^2)\} = 2l_h K_{tm}(Z_M - Z_{O_m})\sin(\sigma - \theta - \theta_m) + 2K_{\theta m}\theta_m + 2C_{\theta m}\dot{\theta}_m - 2\dot{z}\dot{\theta}\{(m_a l_g + m_w l_h)\cos(\sigma - \theta_m)\} - 2U\dot{\theta}\{(m_a l_g + m_w l_h)\sin(\sigma - \theta_m)\} - 2\dot{\theta}^2(m_a l_g + m_w l_h)\{l_b \cos(\sigma - \theta_m) + l_f \sin(\sigma - \theta_m)\}$$

Finally, the fifth equation of the nonlinear model is:

$$2\ddot{z}\{(m_a l_g + m_w l_h)\sin(\sigma - \theta_r)\} + 2\ddot{\theta}\{I_{yw} + I_{ya} + (m_a l_g^2 + m_w l_h^2) + (m_a l_g + m_w l_h)[l_f \cos(\sigma - \theta_r) + l_c \sin(\sigma - \theta_r)]\} - 2\ddot{\theta}_r\{I_{yw} + I_{ya} + (m_a l_g^2 + m_w l_h^2)\} = 2l_h K_{tr}(Z_R - Z_{O_r})\sin(\sigma - \theta - \theta_r) + 2K_{\theta r}\theta_r + 2C_{\theta r}\dot{\theta}_r - 2\dot{z}\dot{\theta}\{(m_a l_g + m_w l_h)\cos(\sigma - \theta_r)\} - 2U\dot{\theta}\{(m_a l_g + m_w l_h)\sin(\sigma - \theta_r)\} + 2\dot{\theta}^2(m_a l_g + m_w l_h)\{l_c \cos(\sigma - \theta_r) - l_f \sin(\sigma - \theta_r)\} \quad (13)$$

By solving simultaneously the five equations in a numerical way, the time responses of this model will be determined.

### 2.2. Linear model

A linear model with 5 degrees of freedom will be presented using the Lagrange modeling method. The assumptions of this model are similar to non-linear model. Due to the linearity of the model and the small angles of motion, it is necessary to disregard the dimensions of the carrying load and the body, and to model these two parts as an integrated beam. Accordingly, the mass and inertia of the



[ DOI: 10.22068/ijae.8.2.2709 ]

body and carrying load will be equivalent in the equations. In Figure 5, two longitudinal distance $l_x$ and a vertical $l_z$ are defined to determine the location of the center of the mass of the equivalent mass, which can be calculated as follows:

$$l_x = \frac{l_c W_b + (l_c + l_m) W_L}{W_b + W_L} \quad (14)$$

$$l_z = \frac{l_f W_b + (l_f + l_k) W_L}{W_b + W_L} \quad (15)$$

Also, $M$ and $I_y$ represent the body and load equivalent mass and inertia, respectively, and can be defined as follows:

$$M = m_b + m_L \quad (16)$$

$$I_y = I_{yb} + I_{yL} + m_b \left[(l_x - l_c)^2 + (l_z - l_f)^2\right] + m_L \left[(l_k + l_f - l_z)^2 + (l_c + l_m - l_x)^2\right] \quad (17)$$

It is necessary to determine the displacement of wheel centers and suspension arms in order to calculate the external forces applied to the suspension system. According to the geometry of the vehicle, the change of the wheel centers is:

$$Z_{O_f} = z + (L - l_x)\theta + l_h(\theta + \theta_f)\sin\sigma \quad (18)$$

$$Z_{O_m} = z + (l_d - l_x)\theta - l_h(\theta + \theta_m)\sin\sigma \quad (19)$$

$$Z_{O_f} = z - l_x\theta - l_h(\theta + \theta_r)\sin\sigma \quad (20)$$

And the travel of the centers of each of the front, middle and rear suspension arms are respectively:

$$Z_{A_f} = z + (L - l_x)\theta + l_g(\theta + \theta_f)\sin\sigma \quad (21)$$

$$Z_{A_m} = z + (l_d - l_x)\theta - l_g(\theta + \theta_m)\sin\sigma \quad (22)$$

$$Z_{A_f} = z - l_x\theta - l_g(\theta + \theta_r)\sin\sigma \quad (23)$$

By differentiation of the above relations, the speed of each of them will also be determined. By changing the location of different parts and the linear and rotational speeds of the vehicle, the kinetic energy, the potential and the damping of the system can be calculated. According to the previous calculations, the kinetic energy of the system will be:

$$\begin{aligned} K = {} & \frac{1}{2}M\dot{z}^2 + \frac{1}{2}I_y\dot{\theta}^2 + \frac{1}{2}(2m_w)\dot{Z}_{O_f}^{\ 2} + \frac{1}{2}(2m_w)\dot{Z}_{O_m}^{\ 2} + \frac{1}{2}(2m_w)\dot{Z}_{O_r}^{\ 2} \\ & + \frac{1}{2}(2m_a)\dot{Z}_{A_f}^{\ 2} + \frac{1}{2}(2m_a)\dot{Z}_{A_m}^{\ 2} + \frac{1}{2}(2m_a)\dot{Z}_{A_r}^{\ 2} + \frac{1}{2}(2I_{yw})(\dot{\theta} + \dot{\theta}_f)^2 \\ & + \frac{1}{2}(2I_{yw})(\dot{\theta} + \dot{\theta}_m)^2 + \frac{1}{2}(2I_{yw})(\dot{\theta} + \dot{\theta}_r)^2 \\ & + \frac{1}{2}(2I_{ya})(\dot{\theta} + \dot{\theta}_f)^2 + \frac{1}{2}(2I_{ya})(\dot{\theta} + \dot{\theta}_m)^2 + \frac{1}{2}(2I_{ya})(\dot{\theta} + \dot{\theta}_r)^2 \end{aligned} \quad (24)$$

And the potential energy of the system is calculated as follows, in which the weight forces and initial displacements of the springs are neglected.

$$\begin{aligned} V = \frac{1}{2}\Big\{ & K_{tf}\left[Z_{O_f} - Z_F\right]^2 + K_{\theta f}\theta_f^2 \\ & + K_{tm}\left[Z_{O_m} - Z_M\right]^2 \\ & + K_{\theta m}\theta_m^2 \\ & + K_{tr}\left[Z_{O_r} - Z_R\right]^2 \\ & + K_{\theta r}\theta_r^2 \Big\} \end{aligned} \quad (25)$$

The system damping energy will be determined as follows, which is related to torsion dampers between each of the three pairs of arms and body.



[ DOI: 10.22068/ijae.8.2.2709 ]

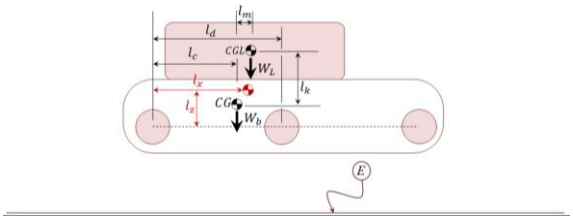

**Figure 5**. Equivalent mass and inertia of the body and load of the vehicle in the linear model of vibrational motion

$$D = \frac{1}{2}\left[(2C_{\theta f})\dot{\theta}_f^2 + (2C_{\theta m})\dot{\theta}_m^2 + (2C_{\theta r})\dot{\theta}_r^2\right] \quad (26)$$

The Lagrange equation will be determined by partial differentiation of the set energy in relation to each of the degrees of the model freedom, and its general relation is:

$$\frac{d}{dt}\left(\frac{\partial K}{\partial \dot{q}}\right) - \frac{\partial K}{\partial q} + \frac{\partial D}{\partial \dot{q}} + \frac{\partial V}{\partial q} = f_r \quad (27)$$

By differentiating, the dynamics equations of the system will be determined as follows. The first equation in this model, which relates to the degree of freedom of body, after simplification is as follows.

$$\begin{aligned}
&\ddot{z}\{M + 6m_a + 6m_w\} + 2\ddot{\theta}\{(m_a + m_w)(L + l_d - 3l_x) - \sin\sigma\,(m_a l_g + m_w l_h)\} \\
&+2(\ddot{\theta}_f - \ddot{\theta}_m - \ddot{\theta}_r)\{\sin\sigma\,(m_a l_g + m_w l_h)\} + 2z\{K_{tf} + K_{tm} + K_{tr}\} \\
&+2\theta\{K_{tf}(L - l_x + l_h \sin\sigma) + K_{tm}(l_d - l_x - l_h \sin\sigma) - K_{tr}(l_x + l_h \sin\sigma)\} \\
&+2l_h \sin\sigma\{\theta_f K_{tf} - \theta_m K_{tm} - \theta_r K_{tr}\} = 2\{K_{tf} Z_F + K_{tm} Z_M + K_{tr} Z_R\}
\end{aligned} \quad (28)$$

The next equation is related to the movement of the pitch angle of the body and can be calculated as follows:

$$\begin{aligned}
&\ddot{z}\{2(L + l_d - 3l_x)(m_a + m_w) - 2\sin\sigma\,(m_a l_g + m_w l_h)\} + \\
&\ddot{\theta}\{I_y + 6I_{ya} + 6I_{yw} + 2m_w[(L - l_x + l_h \sin\sigma)^2 + (l_d - l_x - l_h \sin\sigma)^2 + (l_x + l_h \sin\sigma)^2] + 2m_a\left[(L - l_x + l_g \sin\sigma)^2 + (l_d - l_x - l_g \sin\sigma)^2 + (l_x + l_g \sin\sigma)^2\right]\} \\
&+2\ddot{\theta}_f\{I_{ya} + I_{yw} + \sin\sigma\,(L - l_x)(m_a l_g + m_w l_h) + \sin^2\sigma\,(m_w l_h^2 + m_a l_g^2)\} \\
&+2\ddot{\theta}_m\{I_{ya} + I_{yw} - \sin\sigma\,(l_d - l_x)(m_a l_g + m_w l_h) + \sin^2\sigma\,(m_w l_h^2 + m_a l_g^2)\} \\
&+2\ddot{\theta}_r\{I_{ya} + I_{yw} + \sin\sigma\, l_x(m_a l_g + m_w l_h) + \sin^2\sigma\,(m_w l_h^2 + m_a l_g^2)\} + \\
&2z\{K_{tf}(L - l_x + l_h \sin\sigma) + K_{tm}(l_d - l_x - l_h \sin\sigma) - K_{tr}(l_x + l_h \sin\sigma)\} \\
&+2\theta\{K_{tf}(L - l_x + l_h \sin\sigma)^2 + K_{tm}(l_d - l_x - l_h \sin\sigma)^2 + K_{tr}(l_x + l_h \sin\sigma)^2\} \\
&+2\theta_f\{K_{tf} l_h (L - l_x + l_h \sin\sigma)\sin\sigma\} - 2\theta_m\{K_{tm} l_h (l_d - l_x - l_h \sin\sigma)\sin\sigma\} \\
&+2\theta_r\{K_{tr} l_h (l_x + l_h \sin\sigma)\sin\sigma\} \\
&= 2\{K_{tf}(L - l_x + l_h \sin\sigma) Z_F + K_{tm}(l_d - l_x - l_h \sin\sigma) Z_M - K_{tr}(l_x + l_h \sin\sigma) Z_R\}
\end{aligned}$$

The following equation is related to the front suspension arms and is as follows:

$$\begin{aligned}
&\ddot{z}\{2\sin\sigma\,(m_a l_g + m_w l_h)\} + \\
&2\ddot{\theta}\{I_{yw} + I_{ya} + \sin\sigma\,(L - l_x)(m_a l_g + m_w l_h) + \sin^2\sigma\,(m_w l_h^2 + m_a l_g^2)\} \\
&+2\ddot{\theta}_f\{I_{ya} + I_{yw} + \sin^2\sigma\,(m_w l_h^2 + m_a l_g^2)\} \\
&+2\dot{\theta}_f\{C_{\theta f}\} + 2z\{K_{tf} l_h \sin\sigma\} +
\end{aligned} \quad (30)$$





[ DOI: 10.22068/ijae.8.2.2709 ]

$$2\theta\{K_{tf}l_h(L-l_x+l_h\sin\sigma)\sin\sigma\}+ 2\theta_f\{K_{tf}l_h^2\sin^2\sigma+K_{\theta f}\} = 2\{K_{tf}l_hZ_F\sin\sigma\}$$

The next equation related to the rotation of the middle suspension arms is:

$$\begin{aligned}&\ddot{z}\{2\sin\sigma\,(m_al_g+m_wl_h)\}\\ &-2\ddot{\theta}\{I_{yw}+I_{ya}-\sin\sigma\,(l_d-l_x)(m_al_g+m_wl_h)+\sin^2\sigma\,(m_wl_h^2+m_al_g^2)\}\\ &-2\ddot{\theta}_m\{I_{ya}+I_{yw}+\sin^2\sigma\,(m_wl_h^2+m_al_g^2)\}-2\dot{\theta}_m\{C_{\theta m}\}+2z\{K_{tm}l_h\sin\sigma\}\\ &+2\theta\{K_{tm}l_h(l_d-l_x+l_h\sin\sigma)\sin\sigma\}-2\theta_m\{K_{tm}l_h^2\sin^2\sigma+K_{\theta m}\}\\ &=2\{K_{tm}l_hZ_M\sin\sigma\}\end{aligned} \quad (31)$$

And the final equation related to the movement of the rear suspension arms is:

$$\begin{aligned}&\ddot{z}\{2\sin\sigma\,(m_al_g+m_wl_h)\}-2\ddot{\theta}\{I_{yw}+I_{ya}+\sin\sigma\,l_x(m_al_g+m_wl_h)+\sin^2\sigma\,(m_wl_h^2+m_al_g^2)\}\\ &-2\ddot{\theta}_r\{I_{ya}+I_{yw}+\sin^2\sigma\,(m_wl_h^2+m_al_g^2)\}-2\dot{\theta}_r\{C_{\theta r}\}+2z\{K_{tr}l_h\sin\sigma\}\\ &-2\theta\{K_{tr}l_h(l_x+l_h\sin\sigma)\sin\sigma\}-2\theta_r\{K_{tr}l_h^2\sin^2\sigma+K_{\theta r}\}\\ &=2\{K_{tr}l_hZ_R\sin\sigma\}\end{aligned} \quad (32)$$

As can be seen in the last five equations, the coefficients of each of the state variables in this model are parameters that can be calculated according to the dimensions and masses of the vehicle, and so the equations can be written in the form of space state matrix.

### 2.3. Tires static load

To calculate the static load of the tire, the linear model equations will be used. But, it is necessary to consider the work of weight forces in the amount of potential energy. Accordingly, the amount of potential energy of the system will be:

$$\begin{aligned}V=\frac{1}{2}\Big\{&K_{tf}\left[Z_{O_f}-Z_F\right]^2+K_{\theta f}\theta_f^2+\\ &K_{tm}\left[Z_{O_m}-Z_M\right]^2+K_{\theta m}\theta_m^2+\\ &K_{tr}\left[Z_{O_r}-Z_R\right]^2+K_{\theta r}\theta_r^2\Big\}+Mgz+\\ &2m_wg\left(Z_{O_f}+Z_{O_m}+Z_{O_r}\right)+\\ &2m_ag\left(Z_{A_f}+Z_{A_m}+Z_{A_r}\right)\end{aligned} \quad (33)$$

Taking these terms into account in the potential energy of the car, the value presented in term (34) will be added to the right side of equation (28). Term (35) is also added to the second to the right hand of equation (29). Term (36) will also be combined with the second side of the equation in each of the three equations (30) to (32).

$$-g(M+6m_a+6m_w) \quad (34)$$

$$-2g(m_a+m_w)(L+l_d-3l_x-l_h\sin\sigma) \quad (35)$$

$$-2g\sin\sigma\,(m_al_g+m_wl_h) \quad (36)$$

By simultaneously solving new relations and assuming time derivatives equal to zero, and neglecting the input of the road (according to the principle of virtual work), the amount of static load of the tire will be calculated.

## 3. Simulation

In this section, simulation and comparison of the results of both linear and nonlinear models have been performed. In the following, sensitivity analysis is fully presented for the two models. The geometric parameters of the vehicle for simulation are in accordance with Appendix I.

### 3.1. Comparison of two models results





[ DOI: 10.22068/ijae.8.2.2709 ]

To compare and validate the results of the two models, the base model is moved at 40 km/h on a sinusoidal road maneuver, defined in (1). According to Figure. 6, the period of the road input is 3 seconds and its amplitude is 40 cm, which will be severe maneuver at the indicated speed. In real life, you can estimate a road, with a lot of sinuses with different ranges and periods. Therefore, considering the sinusoidal maneuver can somehow include various maneuvers of the vehicle motion. Depending on the vehicle speed, the value of the central and rear wheels input will follow a certain delay from the front wheel input. This is well illustrated in Figure.6. The time responses provided in this section include five vehicle states and some of the most important parameters of the suspension system including the transmissibility ratio, the dynamic displacement of tire, Suspension travel ratio, and acceleration.

After applying this input, the amount of vehicle suspension transmissibility ratio will be as shown in Figure. 7. The two models are well suited to each other and the major difference is limited to the range of fluctuations at the beginning and the end of the maneuver action. This is due to the greater influence of independent inputs in the nonlinear model, which predicts a more intense fluctuation. A similar process is evident in the amount of velocity 11 of the center of mass as shown in Figure. 8 and shows more serious differences between the two models.

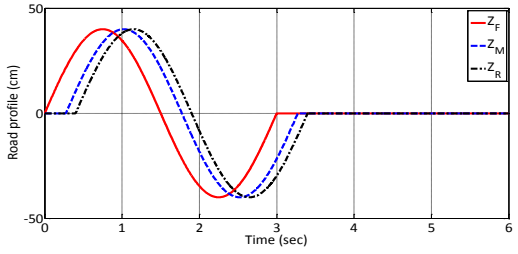


**Figure 6**. Road input profile

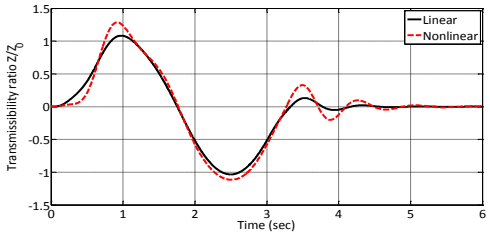


**Figure 7**. Wheel to body transfer ratio

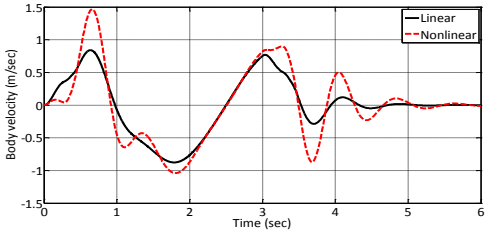


**Figure 8**. Body vertical velocity

Due to the large size of the body moment of inertia compared to the wheels and suspension arms, and all angles changes are in the linear range, the difference in angular response between the two models is very slight and negligible. This is evident in Figure 9 for the body pitch angle.

In the following, the dynamic displacement ratios of each wheel for two linear and nonlinear models are presented in Figures 10 to 12, respectively. First, the responses of the two models are very close together and the models will be verified, and on the other hand, both models follow the road profile well. Dynamic displacement ratio also identifies the forces rise from the road and its range depends on the rigidity of the vehicle tires.

Also, dynamic displacement ratio of the suspension system at the pivot of each of the arms indicates the amount of force transmitted from the unsprung mass to the sprung mass of the vehicle body. The lower the amount of internal power, the better the condition of the vehicle will be in terms of reducing the acceleration in the body. The value of this parameter for each of the front, center, and



[ DOI: 10.22068/ijae.8.2.2709 ]

rear suspensions is shown in Figures 13 to 15, respectively. This parameter will increase in front, back and middle suspension, respectively, and the differences between the two linear and nonlinear models will be approximately the same for all three position.

The angle changes of front suspension arms are as shown in Figure 16. Due to low mass of the arms and the increase of the road input effect in this part of the vehicle, there will be differences in the time response between the two models. In most cases, the amplitude and intensity of oscillations are more severe in the nonlinear model. Similarly, for the middle and rear wheels, figures 17 and 18 are plotted respectively. By moving to the back, the intensity and amplitude of the fluctuations have been increased, and the mid and rear wheels of the vehicle are in a more unfavorable position. Nevertheless, the value of arm rotation in both models is in the range of small angles, which is directly related to the amount of torsional stiffness intended for suspension arms. By reducing the amount of stiffness, the magnitude of these angles will also increase.

In the following, for the vertical load of each of the front, middle, and rear tires of the vehicle, the curve of variation over time is shown in Figures 19-21. It should be noted that the initial load of each tire starts from a static state and then changes according to the road input. The amount of tire vertical load will be calculated using the tire rigidity and displacement. The greatest difference between the two models is at the start and end of the maneuvers, which is gradually damped after the road vibration input is removed. The nonlinear model predicts larger forces for all three tire contact patches.

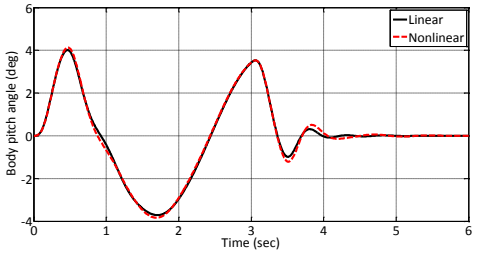


**Figure 9**. Body pitch angle

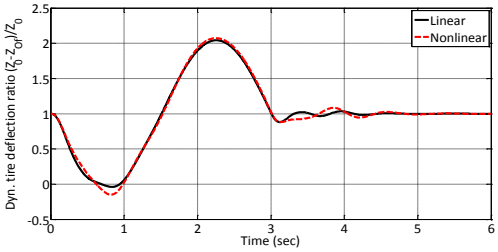


**Figure 10**. Dynamic Tire deflection ratio, front suspension

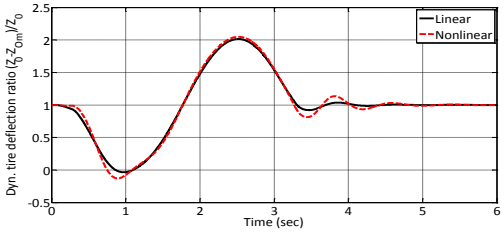


**Figure 11**. Dynamic Tire deflection ratio, middle suspension

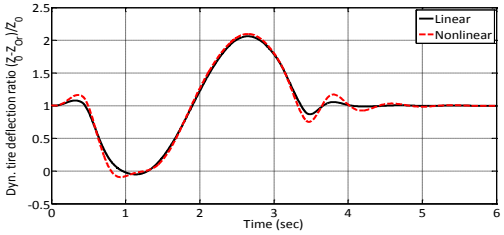


**Figure 12**. Dynamic Tire deflection ratio, rear suspension



[ DOI: 10.22068/ijae.8.2.2709 ]

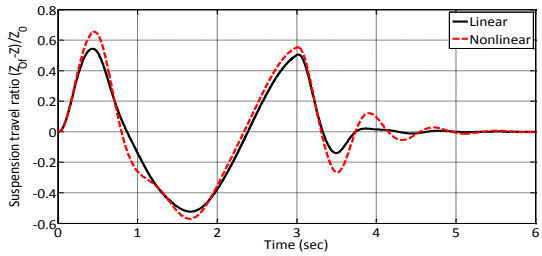


**Figure 13**. Suspension travel ratio, front suspension

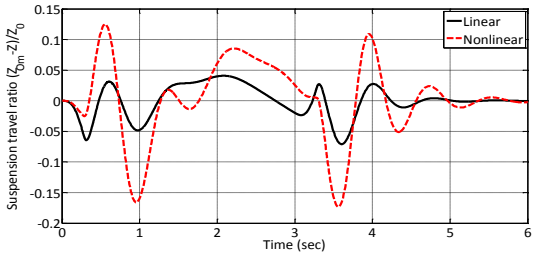


**Figure 14**. Suspension travel ratio, middle suspension

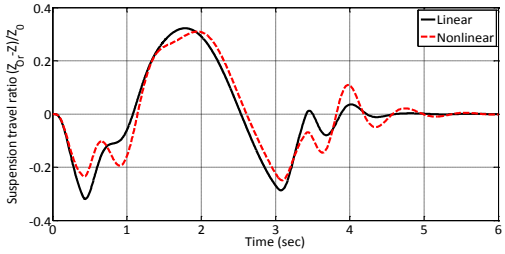


**Figure 15**. Suspension travel ratio, rear suspension

Another important parameter for checking the vibrations of the system is the value of the vertical acceleration of the body and wheel centers. Therefore, the value of the vertical acceleration of the body, and the three wheel center for front, middle and rear wheels are shown in Figures 22 to 25 respectively. The amount of acceleration applied to the body is in the range of 0.6g, which is a significant value. On the other hand, the amount of acceleration in the front, center and rear of the vehicle is in the range of 1.0g, which shows the possibility of separating the tires from the ground. This situation is more critical to the vehicle rear wheels, because the load on the rear axle decreases when the vehicle center of gravity passes through the barrier. Hence, higher vibrations and accelerations will be applied to the rear wheels, and they may sometimes lose their contact to ground by increasing maneuver severity.

According to the explanation, the results of the two models are very close. The main disputes are related to the arms and wheel centers of the suspension system, because they are the vibration entrance, and intermediary parts between road and body, and also are subjected to great forces and moments. One of the reasons for the difference between the two models is the large vibration of the suspension arms relative to the body, because they have less mass and, on the other hand, they are prone to creating great moments due to their deviation from the vertical axis.

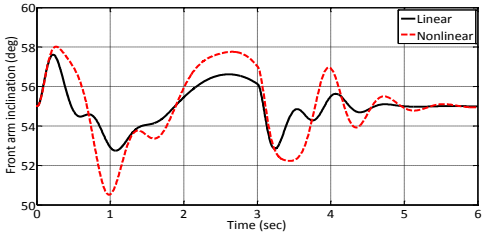


**Figure 16**. Front arm inclination

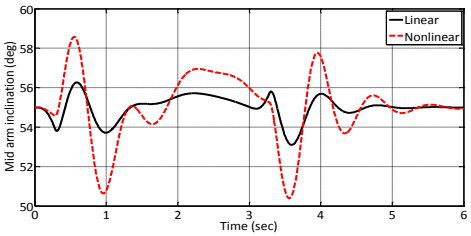


**Figure 17**. Middle arm inclination



[ DOI: 10.22068/ijae.8.2.2709 ]

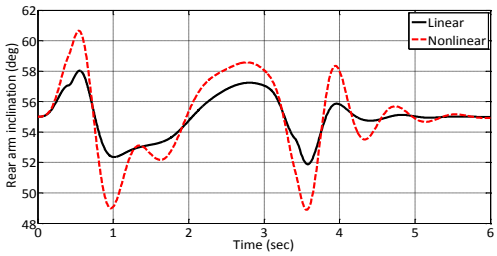


**Figure 18**. Rear arm inclination

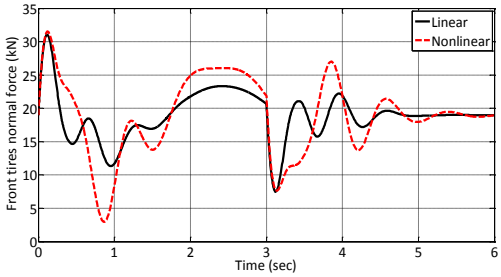


**Figure 19**. Front tire normal force

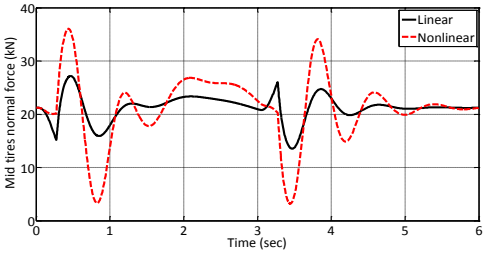


**Figure 20**. Middle tire normal force

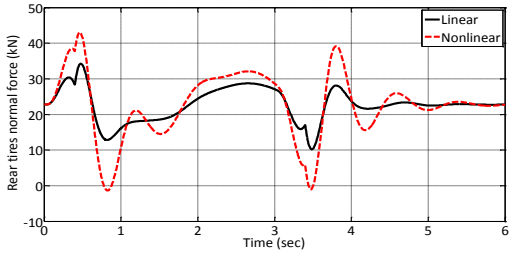


**Figure 21**. Rear tire normal force

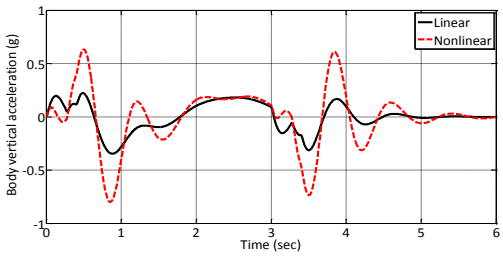


**Figure 22**. Body vertical acceleration

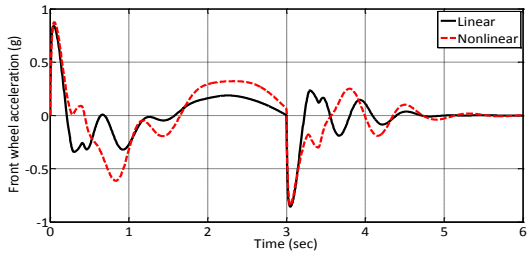


**Figure 23**. Front wheel acceleration

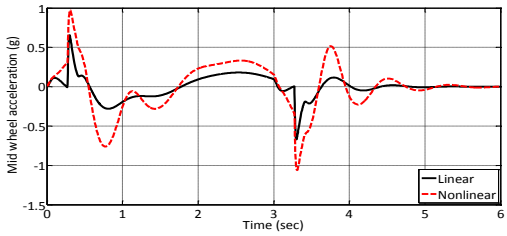


**Figure 24**. Middle wheel acceleration

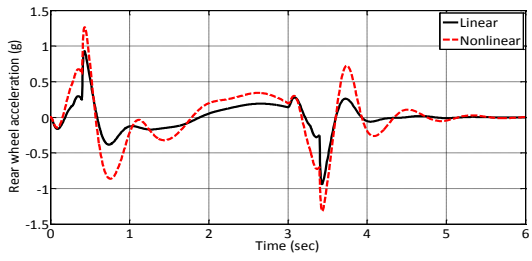


**Figure 25**. Rear wheel acceleration

### 3.2 Sensitivity analysis

In this section, the sensitivity analysis of the important parameters of the rover will be





[ DOI: 10.22068/ijae.8.2.2709 ]

carried out, and in each case, a description will be provided on the significance and type of effect of that parameter. When one of the parameters is selected for sensitivity analysis, the other parameters used for the vehicle will be held constant. The parameters studied in this section include the longitudinal velocity, the initial deviation angle of the suspension arms, body mass, torsional stiffness and damping of the arm and the body joints.

### 3.2.1 Longitudinal velocity effect

The vehicle longitudinal velocity determines the input frequency of the road. Hence, it can stimulate the rover in different modes and change the time response. In Figure 26, Time variations of body transfer ratio is shown, when the vehicle is moving at three different speeds. It will be noted that at low speeds, the amplitude of the oscillations will be shorter and in lower frequencies, and at faster speeds, the amplitude will be higher and the system response is greater. Meanwhile, the behavior of the system from the speed of 30 km/h will not change. Given that the natural frequency of the body pitch angle is small, according to Figure 27, the amount of pitch angle at the lower speeds is greater and the angular oscillations of the body will be reduced by increasing the speed. It should be noted that the longitudinal velocity change is equivalent to changing the frequency profile of the road and can also be considered as an analysis of road entry sensitivity.

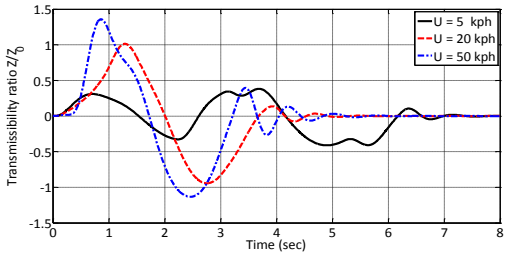


**Figure 26**. Changes in transfer ratio of the suspension due to speed variation

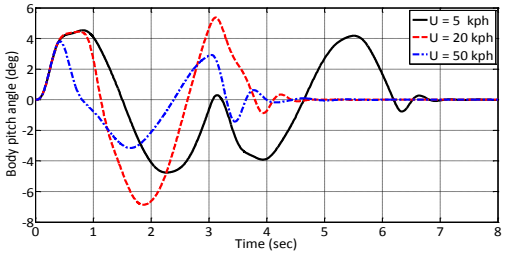


**Figure 27**. Changes in body pitch angle due to speed variation

### 3.2.2 Initial angle of the suspension arms effect

The effect of shifting the angle of the suspension arms on time responses is investigated. As shown in Figures 28 and 29, the angle of 30 degrees as the angle of deviation of the suspended arms causes the transient time response to be unstable, and angles above 50 degrees have no significant effect on the response, and the major effect of this angle increase is the decrease in the height of the center of mass. The reason for unstable responses for small angles is that the angles of the suspension arms are close to zero (vertical). At small angles of the suspension arms, the amount of stabilizing torque by the vertical forces of the tire will be reduced, and in this case, the sensitivity of the vehicle to the longitudinal and vertical vibrations is increased. Accordingly, angles greater than 45 degrees for the suspension arms are suggested to prevent high frequency vibrations in the set.

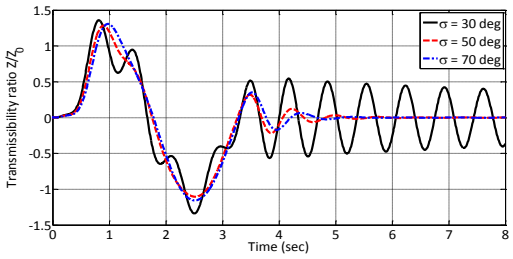


**Figure 28**. Changes in transfer ratio of the suspension due to arms angles variation



[ DOI: 10.22068/ijae.8.2.2709 ]

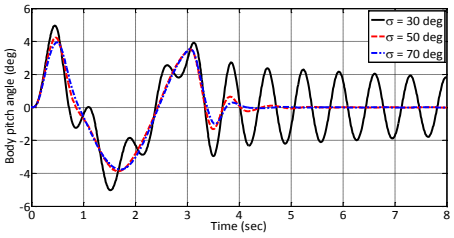


**Figure 29**. Changes in body pitch angle due to arms angles variation

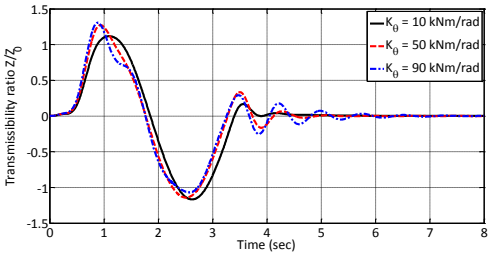


**Figure 32**. Changes in transfer ratio of the suspension due to the spring coefficient variation

### 3.2.3 Vehicle mass effect

The amount of vehicle mass has an effect on the amount of vertical forces of the vehicle tires, that has changed in the order indicated below.

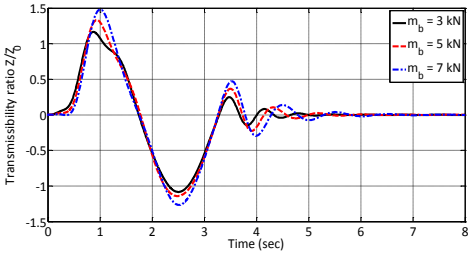


**Figure 30**. Changes in transfer ratio of the suspension due to body mass variation

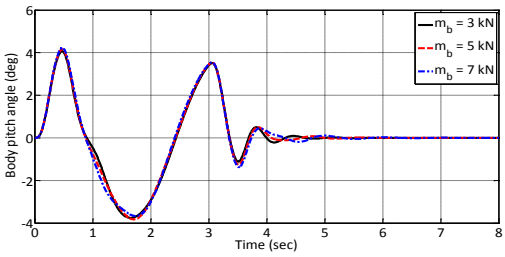


**Figure 31**. Changes in body pitch angle due to body mass variation

Changing the mass of the body can also be a kind of shift in the weight. As shown in Figure 30, by increasing the vehicle mass, the center of mass fluctuation range will increase as the inertia of the system increases, so the natural frequency will decrease. This effect will be negligible on the pitch movement of the body as shown in Figure 31.

### 3.2.4 The torsional stiffness of the spring effect

The torsional stiffness between the arm and body of the vehicle is one of the most important parameters in the vibration analysis. By increasing the stiffness of these springs, the amount of applied forces and moments of the suspension to the body will increase. Therefore it is natural to increase to the amplitude of system fluctuations. This raise in the amplitude of the oscillations is well seen in Figures 32 and 33, even though this toughness increase to the certain values is not effective enough and will not have a significant effect on vehicle time responses.

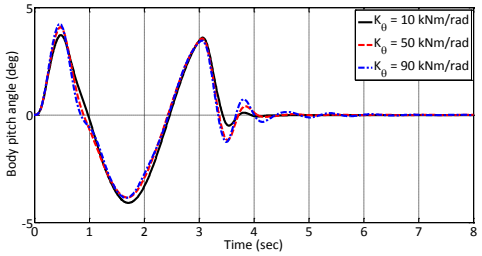


**Figure 33**. Changes in body pitch angle due to the spring coefficient variation

### 3.2.5 Angular damping effect

The angular damping of the suspension arms will have a direct effect on the oscillation and settling time of the vibration. The low amount of angular damping will mount low-range fluctuations on time responses. In Figure. 34,





[ DOI: 10.22068/ijae.8.2.2709 ]

the time variations of the body displacement coefficient for different damping values are presented. By changing in the coefficient of damping from 10 $kN.m.s/rad$ to15$kN.m.s/rad$, a slight effect on the responses is observed. This is evident in the variations in the pitch angle as shown in Figure 35.

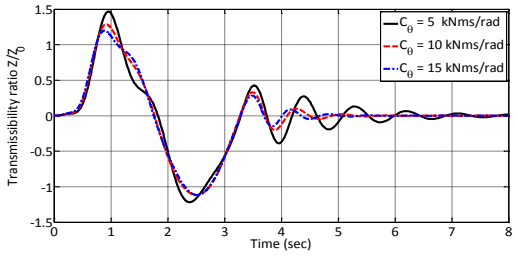


**Figure 34**. Changes in transfer ratio of the suspension due to the damping coefficient variation

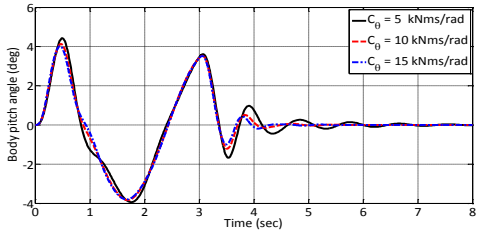


**Figure 35**. Changes in body pitch angle due to the damping coefficient variation

## 4. Conclusions

In this paper, a 5 DOF linear and nonlinear model of a 6 wheeled rover, has been developed. Simulation showed that both linear and nonlinear models often act the same. This type of model has not been proposed by any of author that has been reviewed. In addition some simulations have been executed for both linear and nonlinear models. So the simulations showed the dynamic behavior of the mentioned rover. Finally a sensitivity analysis has been carried out. This analysis can be used in selecting the proper parts of the designed vehicle and define the needed coefficients for example torsional stiffness and damping.

## References

[1] Gilmore, J.M., *The army's future combat systems program and alternatives*. 2006, United States: Congressional Budget Office (CBO).

[2] http://defense-update.com/20140818_collaborative_robotic_test.html. *US Army, Lockheed Martin Test Collaborative Robotics at Ft Benning*. [cited 2017.

[3] http://archive.armytimes.com/article/20110815/NEWS/108150336/Army-kills-off-MULE-unmanned-vehicle. [cited 2014 12 Dec].

[4] https://en.wikipedia.org/wiki/Multifunctional_Utility/Logistics_and_Equipment_vehicle. *Multifunctional Utility/Logistics and Equipment vehicle*. [cited 2017.

[5] Millard, F.R., A. Raj, E.A. David, T.F. John, L.C. Robert, J.L. Robert, and M. Jim, *Technology development for army unmanned ground vehicles*. 2003, Washington, D.C.: National Academies Press (NAP).

[6] Gwaltney, G., *MULE: Multifunctional Utility, Logistics and Equipment Vehicle*. 2012, MichiganTech: Keweenaw Research Center.

[7] Chun, W.H., M.S. Beck, J.T. Stinchcomb, D.A. Clemens, J.C. Dunne, and E.N. Anderfaas, *Articulated vehicle suspension system shoulder joint*. 2007, Google Patents.

[8] Fauroux, J.-C., F. Chapelle, and B. Bouzgarrou. *A new principle for climbing wheeled robots: serpentine climbing with the open-wheel platform*. in *Intelligent Robots and Systems, 2006 IEEE/RSJ International Conference on*. 2006. IEEE.

[9] Seidla, A. *Actively articulated suspension for a four-wheeled vehicle*. in *DS 50: Proceedings of NordDesign*



[ DOI: 10.22068/ijae.8.2.2709 ]

*2008 Conference, Tallinn, Estonia, 21.-23.08. 2008*. 2008.

[10] Fauroux, J., M. Forlorou, B. Bouzgarrou, and F. Chapelle. *Design and modeling of a mobile robot with an optimal obstacle-climbing mode*. in *Proc. 2nd World Congress in Design and Modelling of Mechanical Systems, CMSM*. 2007.

[11] Miller, D.P. and T.-L. Lee, *High-speed traversal of rough terrain using a rocker-bogie mobility system.* Space, 2002.

[12] Bickler, D.B., *Articulated Suspension System*. 1989, Google Patents: US Patent Office, Washington, D. C.

[13] Bickler, D.B., *The new family of JPL planetary surface vehicles.* Missions, Technologies, and Design of Planetary Mobile Vehicles, 1993. **1**: p. 301-306.

[14] Avinash, S., V. Anurag, A. Singh, S. Shah, and K. Krishna. *A semi-active robot for steep obstacle ascent*. in *Control Applications (CCA), 2013 IEEE International Conference on*. 2013. IEEE.

[15] Iagnemma, K., A. Rzepniewski, S. Dubowsky, and P. Schenker, *Control of robotic vehicles with actively articulated suspensions in rough terrain.* Autonomous Robots, 2003. **14**(1): p. 5-16.

[16] Lauria, M., Y. Piguet, and R. Siegwart. *Octopus: an autonomous wheeled climbing robot*. in *Proceedings International Conference on Climbing and Walking Robots*. 2002.

[17] Volpe, R., J. Balaram, T. Ohm, and R. Ivlev. *The rocky 7 mars rover prototype*. in *Intelligent Robots and Systems' 96, IROS 96, Proceedings of the 1996 IEEE/RSJ International Conference on*. 1996. IEEE.

[18] Leppänen, I., S. Salmi, and A. Halme. *WorkPartner–HUT-Automations new hybrid walking machine*. in *1st International Conference on Climbing and Walking Robots, Brussels*. 1998.

[19] Rollins, E., J. Luntz, A. Foessel, B. Shamah, and W. Whittaker. *Nomad: a demonstration of the transforming chassis*. in *Robotics and Automation, 1998. Proceedings. 1998 IEEE International Conference on*. 1998. IEEE.

[20] Kemurdjian, A. *Planet rover as an object of the engineering design work*. in *Robotics and Automation, 1998. Proceedings. 1998 IEEE International Conference on*. 1998. IEEE.

[21] Lim, K.B., S. Park, S. Kim, J.M. Jeong, and Y.-S. Yoon. *Behavior planning of an unmanned ground vehicle with actively articulated suspension to negotiate geometric obstacles*. in *Intelligent Robots and Systems, 2009. IROS 2009. IEEE/RSJ International Conference on*. 2009. IEEE.

[22] Kang, J., W. Kim, S. Jung, J. Lee, and K. Yi. *Skid steering based autonomous driving of Robotic Vehicle with Articulated Suspension*. in *ICCAS-SICE, 2009*. 2009. IEEE.

[23] Kang, J., W. Kim, J. Lee, and K. Yi, *Skid steering-based control of a robotic vehicle with six in-wheel drives.* Proceedings of the Institution of Mechanical Engineers, Part D: Journal of Automobile Engineering, 2010. **224**(11): p. 1369-1391.

[24] Kang, J., W. Kim, J. Lee, and K. Yi, *Design, implementation, and test of skid steering-based autonomous driving controller for a robotic vehicle with articulated suspension.* Journal of mechanical science and technology, 2010. **24**(3): p. 793-800.

[25] Bares, J., S. McFadden, T. Stentz, C. Richards, and S. Murray. *Designing crash-survivable unmanned vehicles*. in *Proceedings of the AUVSI Unmanned Systems 2002 Conference, Orlando*. 2002.

[26] Fauroux, J., P. Vaslin, and G. Douarre. *Improving skid-steering on a 6x6 all-terrain vehicle: A preliminary experimental study*. in *Proc. of*



[ DOI: 10.22068/ijae.8.2.2709 ]

*IFToMM 2007, The 12th World Congress in Mechanism and Machine Science*. 2007.

[27] Javed, M.A., *A State Estimation Approach for a Skid-Steered Off-Road Mobile Robot.* 2013.

[28] Sanan, S., *Controlling an actively articulated suspension.* Advances in Climbing and Walking Robots: p. 81.

[29] Eathakota, V.P., S. Kolachalama, A.K. Singh, and K.M. Krishna, *Force Actuator based Articulated Suspension Vehicle for Rough Terrain Mobility*.

[30] Kane, T.R. and D.A. Levinson, *Dynamics, Theory and Applications*. 1985: McGraw-Hill.



[ DOI: 10.22068/ijae.8.2.2709 ]